The Influence of Equation of State on the Giant Impact Simulations

Hosono, Natsuki

Karato, Shun-ichiro

(Citation)
Journal of Geophysical Research: Planets,127(6):e2021JE006971

(Issue Date)
2022-06

(Resource Type)
journal article

(Version)
Version of Record

JGR Planets

RESEARCH ARTICLE
10.1029/2021JE006971

The Influence of Equation of State on the Giant Impact Simulations

Natsuki Hosono[1,2,3] and Shun-ichiro Karato[4]

[1]Department of Planetology, Kobe University, Kobe, Japan, [2]RIKEN Center for Computational Science, Kobe, Japan, [3]Japan Agency for Marine-Earth Science and Technology, Yokohama, Japan, [4]Department of Earth and Planetary Sciences, Yale University, New Haven, CT, USA

Key Points:

- We surveyed the effect of equation of state for Earth's mantle on mantle ejection by a canonical Moon-forming impact model
- The use of modified hard-sphere equations of state (EoS) for the magma ocean provides a reasonable explanation for the composition of the Moon
- The EoS that treats the solid and liquid in a similar way cannot explain the composition of the Moon

Correspondence to:
N. Hosono,
natsuki.hosono@crystal.kobe-u.ac.jp

Citation:
Hosono, N., & Karato, S.-i. (2022). The influence of equation of state on the giant impact simulations. *Journal of Geophysical Research: Planets*, *127*, e2021JE006971. https://doi.org/10.1029/2021JE006971

Received 7 JUN 2021
Accepted 17 MAY 2022

Abstract We explore the role of various equations of state (EoS) in controlling the composition of the Moon formed by a giant impact (GI) using a density-independent SPH code. A limitation in our previous model Hosono et al. (2019), https://doi.org/10.1038/s41561-019-0354-2 is improved by replacing the EoS of the solid from Tillotson EoS to M-ANEOS, and we also explored two recently proposed EoSs by Stewart et al. (2020), https://doi.org/10.1063/12.0000946 and Wissing and Hobbs (2020a), https://doi.org/10.1051/0004-6361/201935814; Wissing and Hobbs (2020b), https://doi.org/10.1051/0004-6361/201936227. The goal is to investigate to what extent we can explain the observed composition of the Moon including the similarity in the isotopic composition and the dissimilarity in the FeO/(FeO + MgO) ratio as compared to that of Earth by the different types of EoS assuming the conventional collision conditions. We found that changing the EoS for solids from Tillotson to M-ANEOS EoS resolves the issues of latent heat, but its effect on the composition of the disk is small compared to the influence of the hard-sphere EoS of magma ocean in controlling the composition of the disk. Similarly, two recently proposed EoSs have small effects on the composition of the disk in comparison to the model where the hard-sphere EoS is used for preexisting magma ocean. We attribute this difference to a fundamental difference in thermodynamic behavior of silicate melts captured by the hard-sphere EoS and by newly proposed EoSs; in the hard-sphere model of silicate melts, configurational entropy dominates in free energy, whereas in the newly proposed model, entropy is dominated by vibrational entropy similar to entropy of solids.

Plain Language Summary Explaining the observed close similarities in the isotopic compositions of the Moon and Earth is a big challenge in planetary science. Many models invoke unconventional collision conditions but their plausibility is questionable. In our recent paper, we explored an alternative model where we assume a conventional collision condition but use recently developed new types of equation of state for melts, assuming that the magma ocean (MO) covered the growing Earth on which a giant impact occurred. In the present paper, we extend our previous work in modifying the equation of state of solid and also tested two new types of equations of state. We conclude that the modification of the equation of state for solid does not make a large difference in the composition of the Moon and that the recently proposed new equations of state fail to explain the composition of the Moon. We conclude the magma ocean on the growing Earth played a major role to control the composition of the Moon similar to that of Earth, and for the magma ocean, an equation of state that captures the unique thermodynamic properties of silicate melts needs to be used.

1. Introduction

The giant impact (GI) hypothesis is a well-accepted hypothesis for the origin of the Moon that can explain the large angular momentum of the Moon-Earth system and the rocky composition of the Moon within a plausible range of collision conditions (e.g., Canup, 2014; Canup & Asphaug, 2001; Elkins-Tanton, 2013; Halliday, 2012; Melosh, 2014; Stevenson, 1987). However, explaining the similar isotopic compositions of the Moon and Earth by this model is challenging because most models showed that the Moon is mostly made of impactor rather than Earth (e.g., Canup, 2004) (regarding the isotopic observations, see sections III and IV of the Supplementary Information in Hosono et al.,. 2019). Consequently, many models were proposed where rare collision conditions, such as a head-on collision of similar mass planets or an extremely high energy collision, are invoked to explain the similarity in the isotopic compositions (for a review, see Canup et al., 2021). In addition, any successful model must also explain the observed difference in the major element composition between the Moon and Earth (e.g., higher FeO/MgO for the Moon than for Earth; Melosh, 2014; Sakai et al., 2014). However, in most of the previous

studies, the similarity in isotopic compositions is emphasized and there is not much attention to the difference in the FeO/MgO ratio (except for Wissing and Hobbs [2020a] and Pahlevan et al. [2011]).

Noting the fundamental differences in the thermodynamic properties of silicate melts and solids, Karato (2014) showed that when a melt and a solid collide, a melt is much more heated than a solid and proposed that when a giant impact occurs on a planet covered by a magma ocean, then the disk will be made mostly of the magma ocean materials from the target (a growing planet). Since the melt formed from solids contains a larger amount of FeO, this model also explains the difference in the FeO/MgO ratio between the Moon and Earth together with the similarity in the isotopic ratio.

This model was explored in detail by Hosono et al. (2019) where they also tested the consequence of different schemes of SPH including a modified SPH to deal with the issue of a density discontinuity (DISPH; Hopkins, 2013; Hosono et al., 2013; Saitoh & Makino, 2013). They showed that if a hard-sphere EoS is used for the preexisting magma ocean of the growing Earth together with DISPH, then the similar isotopic composition between the Moon and Earth and the higher FeO content than Earth can be explained for a reasonable range of impactor materials with conventional collision conditions. If a conventional SPH is used, no model can explain the composition of the Moon with canonical collision conditions.

However, recently, Stewart et al. (2020) pointed out that the use of the Tillotson EoS for solids by Hosono et al. (2019) leads to a problem in evaluating the latent heat upon a phase change from solids to gas and proposed a modified EoS that is supposed to be able to treat all three phases of a material in a consistent way (see our comments on this equation of state in the next section). They did it by introducing a few parameters in the M-ANEOS EoS and explored its consequences for a GI modeling. Also, Wissing and Hobbs (2020b) and Wissing and Hobbs (2020a) proposed a new EoS with the emphasis on the Grüneisen parameter and explored its influence on the outcome of a GI.

In this paper, we extended our previous study in a few ways. First, we extended our previous study (Hosono et al., 2019) (a) by using the M-ANEOS equation of state for the solid part to rectify the inconsistency of using the (Tillotson, 1962) for the solid part and the hard-sphere EoS for the magma ocean part and (b) we investigate the influence of temperature and density dependence of hard-sphere radii (i.e., a "soft-sphere" model). Second, we explore newly proposed equations of state for the giant impact simulation, including the ones by Stewart et al. (2020) and the one by Wissing and Hobbs (2020b); Wissing and Hobbs (2020a) using DISPH.

In order to focus on the influence of different equations of state, we use the same initial conditions for the target (protoplanet) for all runs containing a magma ocean on the top 1,500 km thick but solids below. For the solid part, we use the same or similar equation of state, but we use different equations of state (mostly M-ANEOS) for the magma ocean including a case where the same EoS (i.e., M-ANEOS) is used for both the magma ocean on the top of the target and the solid materials below.

Even for the initially solid part on the target (and the impactor), some melting will occur after an impact. However, when a magma ocean is present, then a majority of heating is in the magma ocean as shown by Karato (2014), and the degree of melting in the initially solid parts is limited as we will show later.

This paper is organized as follows. In Section 2, we briefly review some basics of equation of state with the emphasis on the unique thermodynamic properties of silicate (and oxide) melts. In Section 3, we briefly introduce the numerical method and analysis. In Section 4, we show the results. In Section 5, we summarize the results and provide a discussion to interpret the results.

2. Equation of State

The use of appropriate equation of state (EoS) is important in a giant impact simulation. Equation of state is a functional relation between the density of a matter with temperature and pressure and contains an essential feature of the change in thermodynamic properties of matter upon an impact. The fundamental thermodynamic identity for the equation of state is

$$p = -\left(\frac{\partial F}{\partial V}\right)_T = -\left(\frac{\partial U}{\partial V}\right)_T + T\left(\frac{\partial S}{\partial V}\right)_T = p_0 + p_{\rm th}, \quad (1)$$

where p is pressure, T is temperature, F is Helmholtz free energy ($F = U - TS$), U is internal energy, S is entropy, and $p_0 = -\left(\frac{\partial U}{\partial V}\right)_T$ and $p_{\rm th} = T\left(\frac{\partial S}{\partial V}\right)_T$. Entropy, S, is a measure of disorder of a material and plays a major role in controlling the degree of heating upon compression (collision). Entropy can be classified into vibrational entropy ($S_{\rm vib}$) and configurational entropy ($S_{\rm conf}$). In a solid where mean atomic positions are fixed, the dominant contribution to entropy is entropy caused by the small deviation of atomic positions around the mean positions due to lattice vibration (i.e., vibrational entropy, $S_{\rm vib}$). In a gas or a liquid, interatomic forces are weak and atoms change their positions much more than in solids and entropy is much larger than that in solids. Entropy due to the change in atomic positions compared to or exceeding the mean atomic distance is called configurational entropy ($S_{\rm conf}$). Since such an extensive displacement of atoms occurs due to weak interatomic forces, the link between configurational entropy and internal energy is weak. This makes a big difference in the thermodynamic properties between solids and fluids (gas and liquid); upon compression, much more heat is produced in a liquid than in a solid (Karato, 2014) and hence initially liquid materials expand a lot more than initially solid materials, and the initially liquid materials would make an important part of the disk.

When chemical bonding among atoms (or ions) plays an important role, internal energy plays a dominant role, and the entropy term plays a secondary role ($p_0 \gg p$th). This is a case for solids where atoms are located near their stable positions. In such a case, entropy is mainly from atomic vibration, that is, vibrational entropy ($S_{\rm vib}$), and since atomic vibration is controlled by chemical bonding, $S_{\rm vib}$ is closely linked to internal energy (U). In such a case, Equation 1 can be written as

$$p = p_0 + \frac{\gamma}{V} U_{\rm th}, \tag{2}$$

where $\gamma = \frac{\partial \log \omega}{\partial \log \rho}$ is the Grüneisen parameter and ω is the vibrational frequency of atoms that is closely connected to the chemical bonding, that is, U. This type of equation of state is called the Mie-Grüneisen equation of state. Note that although this type of equation of state is valid only for solids, in a newly proposed "universal" equation of state by Stewart et al. (2020), they use this type of equation of state for a liquid.

Chemical bonding (interatomic potential) depends on the interatomic distance. In a simple case where interatomic potential depends only on the interatomic distance (central force), the Birch's law of correspondent state follows and one can predict that the Grüneisen parameter decreases with compression as $\frac{\gamma}{\gamma_0} = \frac{V}{V_0}$ (e.g., Anderson, 1996). Another prediction of this type of equation of state is that the bulk modulus (resistance for compression) depends strongly on chemical composition.

Experimental observations on compression of silicate and oxide melts show major deviations from these predictions: bulk moduli of silicate or oxide melts are nearly independent of composition and the Grüneisen parameter increases with compression (e.g., Jing & Karato, 2011) (see also Hosono et al. (2019) (Supporting Information)). This suggests that the thermodynamics of compression of these liquids is fundamentally different from that of solids, and the equation of state for silicate and/or oxide melts cannot be developed by the modifications of the Mie-Grüneisen equation of state. An appropriate equation of state for a silicate melt must capture this essential feature. The key the experimental observations are (a) nearly compositionally independent bulk moduli and (b) strong dependence of sound velocities (i.e., bulk moduli) on frequency suggests that a change in (configurational) entropy plays a key role in the compression of silicate melts.

The hard-sphere equation of state was proposed for the EoS of silicate and oxide melts based on these observations. The hard-sphere EoS starts from the equation of state of an ideal gas (rather than starting from the equation of state of solids) where the entropy rather than the internal energy dominates and the entropy is mostly configurational entropy (the entropy related to the change in the configuration of hard spheres) rather than the vibrational entropy. Therefore, in these liquids, thermal pressure comes mostly from the configurational entropy (not the vibrational entropy), $p_{\rm th} = T\left(\frac{\partial S_{\rm conf}}{\partial V}\right)_T$ and pth $\gg p_0$. Consequently, upon a collision, most of the energy is converted to the thermal energy that results in intense heating. This type of equation of state explains all the major experimental observations on the compression of these liquids, including the increase in the Grüneisen parameter with compression, although some modifications are needed to introduce deformability of hard spheres (e.g., Jing & Karato, 2011).

One issue in using the equation of state in a giant impact simulation is that since a very broad P-T range is involved upon a giant impact, equations of state that can describe the compressional behavior of materials under the broad conditions are needed, including solid, liquid, and gas. For different phases (say liquid and solid), different equations of state need to be used and the discontinuity in some properties, such as density and entropy, needs to be specified properly (presence of discontinuities in density raises an important technical issue of computation of the consequence of a giant impact. A commonly used SPH code contains a physically unreasonable equation that generates an artificial surface tension (Hosono et al., 2013; Saitoh & Makino, 2013) that results in the limited amount of mass ejected by an impact).

In the following, we discuss some key features of equations of state used in the present study, including M-ANEOS (Melosh, 2007), modified M-ANEOS (Stewart et al., 2020), Wissing and Hobbs (2020b); Wissing and Hobbs (2020a) model, and a revised Hosono et al. (2019) model. Details of M-ANEOS (Melosh, 2007) and the modified hard-sphere EoS (Hosono et al., 2019; Jing & Karato, 2011) are given by original papers. Here, we provide a brief explanation of newly proposed EoS, including modified M-ANEOS.

In this paper, we used the Tillotson EoS for iron core for all runs. We used M-ANEOS (with and without Stewart et al. (2020)'s modification) or Wissing and Hobbs (2020b) EoS for the solid rock. Below, we will briefly review some basics of these EoSs.

2.1. Modified M-ANEOS (Stewart et al., 2020)

Stewart et al. (2020) modified the M-ANEOS and introduced a parameter to deal with the discontinuity in some thermodynamic parameters upon a solid to gas phase transformation. In ANEOS, the influence of a phase transformation from a solid to a gas is dealt with by generalizing the thermal part ($F\mathrm{th} = -TS$) of the Helmholtz free energy to

$$F_{\mathrm{th}}(\rho, T) = F_{\mathrm{D}}(\rho, T) + F_{\mathrm{con}}(\rho, T), \tag{3}$$

where F_{D} is the thermal Helmholtz energy corresponding to the Debye model and F_{con} is the "connector" between the Debye model (appropriate for solids) and the ideal gas. They are given by

$$F_{\mathrm{D}}(\rho, T) = n_0 k_{\mathrm{B}} T f_{\mathrm{cv}} \left\{ 3\log\left[1 - \exp\left(-\frac{T_{\mathrm{D}}}{T}\right)\right] - \mathcal{D}\left(\frac{T_{\mathrm{D}}}{T}\right)\right\}, \tag{4}$$

$$F_{\mathrm{con}}(\rho, T) = \frac{3}{2b} n_0 k_{\mathrm{B}} T \log\left(1 + \Psi^b\right), \tag{5}$$

$$\Psi(\rho, T) = Z(\rho, T)\frac{C_{13}\rho^{2/3}T}{T_{\mathrm{D}}^2}, \tag{6}$$

$$C_{13} = \frac{n_0^{5/3}h^2}{2\pi k_{\mathrm{B}}} \exp\left\{\frac{2}{3}\sum_a \frac{n_a}{n_0}\log\left(\frac{n_a}{n_0^{5/3}m_a}\right)\right\}, \tag{7}$$

$$T_{\mathrm{D}}(\rho) = \begin{cases} T_{\mathrm{D0}}\left(\frac{\rho}{\rho_0}\right)^{2/3} \exp\left\{\gamma_0\left(1 - \frac{\rho}{\rho_0}\right) - \frac{1}{3}\left[3 - 4\frac{\rho_0}{\rho} + \left(\frac{\rho_0}{\rho}\right)^2\right]\right\} & (\rho > \rho_0), \\ T_{\mathrm{D0}}\frac{\rho}{\rho_0}\exp\left[\frac{1}{2}(1 - 2\gamma_0)\left(\frac{\rho}{\rho_0}\right)^2 + (3\gamma_0 - 2)\frac{\rho}{\rho_0} - 2\gamma_0 + \frac{3}{2}\right] & (\rho \le \rho_0). \end{cases} \tag{8}$$

Where n_0 is the average number of atoms per unit volume, k_{B} is the Boltzmann constant, T_{D} is the Debye temperature that depends on the density ρ, h is the Plank constant, n_a is the number of atoms with atomic mass m_a, and ρ_0 is the reference density. The function $\mathcal{D}$ is the third-order Debye integral. The function Ψ connects the Debye model to the ideal gas at the limit of low density ($\rho \to 0$) or high temperature ($T \to \infty$). The parameter b is a parameter to modify critical point. In this paper, following Melosh (2007), we chose $b = 0.5$. $Z(\rho, T)$ is the effect of molecular cluster (Melosh, 2007). The parameter f_{cv} is a parameter to adjust the specific heat capacity in the gas region (Stewart et al., 2020).

Table 1
Tables for the Parameters for Each EoS

M-ANEOS										
	ρ_0 (kg/m^3)			γ_0			T_{D0}			f_{cv}
Dunite[a]	3,320			0.82			676			1.0
Dunite[b]	3,220			0.65			1,300			1.35
Hard-sphere EoS										
	ρ_0(kg/m^3)			σ_0(nm)			T_0(K)		η	ξ
MgO[c]	2,650			0.2627			1,673		0.00	0.22
SiO_2[c]	2,650			0.3356			1,673		−0.02	0.62
Wissing and Hobbs EoS										
	ρ_0(kg/m^3)	B(GPa)	B'	t_{min}	δ_t	a_{Mie}	b_{Mie}	c	γ_0	q_0
Solid[d]	3,300	130	4.2	2.2	13	5.924	5/3	0.77	1.2	2.25
Liquid[e]	2,800	23	6.2	2.2	0	5.924	5/3	0.77	2.2	−0.17

[a]Thompson et al. (2019). [b]Stewart et al. (2019). [c]Jing and Karato (2011). [d]Wissing and Hobbs (2020b). [e]Wissing and Hobbs (2020a).

An important limitation of this EoS is not adequately included: both solid and liquid states are described by the same equation of state, that is, the Mie-Grüneisen EoS where only the vibrational entropy is considered. The serious limitation of this type of equation of state in investigating the consequence of a giant impact was discussed by Hosono et al. (2019) and Karato (2014).

Another limitation of this EoS is that the density dependence of Grüneisen parameter is not treated in any detail (see Equation 4). The parameter f_{cv} is assumed to be constant (density independent) in their model. f_{cv} corresponds to γ/V and for solids $\gamma \propto V$ and therefore, the assumption of a constant f_{cv} is approximately valid for solids but not for liquids. For silicate melts, density dependence of the Grüneisen parameter is opposite, that is, $\gamma \propto q$ with $q < 0$ (e.g., Jing & Karato, 2011; Mosenfelder et al., 2007). The volume dependence of the Grüneisen parameter has a strong effect on shock heating (Karato, 2014), and this limitation has an important consequence for the outcome of a giant impact.

We used this modified M-ANEOS to conduct giant impact simulations in the initially solid part of our model, while the equation of state for the magma ocean part is the hard-sphere equation of state. In a model calculation testing by Stewart et al. (2020), we use M-ANEOS (modified version) for both initial magma ocean and initial solid parts. The parameters used in these simulations are summarized in Table 1. For model A (classic M-ANEOS for all materials), we used the input table provided by Thompson et al. (2019). For model B (modified M-ANEOS for all materials), we used the input table provided by Stewart et al. (2019). Note that the input table provided by Thompson et al. (2019) includes a solid-solid phase transition, whereas that provided by Stewart et al. (2019) does not. On the other hand, the input table provided by Stewart et al. (2019) includes melt transition, whereas that provided by Thompson et al. (2019) does not. However, as we have mentioned above, M-ANEOS utilizes the same equation of state for the liquid phase, leading to the inadequate treatment of the uniqueness of the liquid phase.

M-ANEOS is a complex and computationally expensive EoS. In this paper, we create a lookup table of pressure (and sound speed) on the density-temperature grid generated by a public code (Stewart et al., 2019; Thompson et al., 2019). We set the number of density points and temperature points to 860 and 744, respectively. To obtain pressure between data points in a lookup table, we used the linear interpolation method on both density and temperature. Note that the results of simulations with M-ANEOS may depend on the number of grid points or the interpolation method. However, we believe that the effect is less significant than the effect of the type of EoS.

2.2. The Hard-Sphere EoS

The hard-sphere EoS is developed for complex melts, such as silicate melts, based on three experimental observations. (a) The bulk moduli of silicate melts have weak correlation with those of the corresponding solids and assume nearly constant value (K = 20–30 GPa at P < 1 GPa) (Hosono et al., 2019; Jing & Karato, 2011), (b) the sound velocity $c = \sqrt{K/\rho}$ (K: bulk modulus, ρ: density) is a strong function of frequency (Rivers & Carmichael, 1987), and (c) the Grüneisen parameter increases with compression (decreases with volume) as opposed to the behavior in solids (Jing & Karato, 2011; Mosenfelder et al., 2007). These observations suggest that the compression mechanisms of silicate melts are completely different from those of solid silicates.

From the thermodynamical point of view, these observations imply that upon compression of silicate melts, internal energy does not change much and rather a majority of compression occurs by the geometrical rearrangement of hard spheres (groups of atoms, such as MgO, SiO_2). In other words, compression of such a liquid is associated with a change in the entropy (the configurational entropy). Consequently, this model starts with the thermodynamic identity,

$$p = -\left(\frac{\partial F}{\partial V}\right)_T \sim T\left(\frac{\partial S}{\partial V}\right)_T, \tag{9}$$

where S is the configurational (not vibrational) entropy. To calculate the configurational entropy, we start from a model similar to the van der Waals model of nonideal gas where the role of the exclusive volume is introduced. By extending such a model to a high density of "hard spheres," we can write a hard-sphere equation of state (Thiele, 1963) modified for multiple species by Lebowitz et al. (1965) as,

$$p = \frac{RT}{V}\frac{1 + A_1 f + A_2 f^2}{(1-f)^3}, \tag{10}$$

where f is the volume fraction of hard spheres and A_1 and A_2 are the correction factors for the presence of several hard spheres that depend on the diameters (σ_i) of spheres and their concentrations (X_i).

As one can see from Equation 10, it is an extension of the equation of state of an ideal gas (as $f \to 0$, the EoS becomes $p = \frac{RT}{V}$). Consequently, this EoS describes a continuous change in the state from a liquid to a gas state and therefore, there is no issue of the latent heat if the P-T conditions after a giant impact exceed the critical points (p_c, T_c).

In this paper, we make two modifications to the EoS from the hard-sphere EoS (Hosono et al., 2019; Jing & Karato, 2011). Rather than a fixed size of a hard-sphere, we use a deformable sphere model, where the hard-sphere radius (σ) changes with temperature and density as Jing and Karato (2011),

$$\sigma = \sigma_0\left(\frac{T}{T_0}\right)^{\eta}\left(\frac{\rho}{\rho_0}\right)^{-\xi/3}, \tag{11}$$

where σ_0, T_0, and ρ_0 are the reference values for the hard-sphere radius, temperature, and density, respectively. The power indices η and ξ are temperature and volume dependence of hard-sphere radii. Then, the pressure and specific internal energy (u) can be written as

$$p = \frac{N_{\mathrm{HS}}\bar{R}}{\bar{M}}(1-\xi)\Phi(f)\rho T, \tag{12}$$

$$u = \frac{N_{\mathrm{HS}}\bar{R}}{\bar{M}}\left\{\frac{3}{2} + 3\eta\left[\Phi(f) - 1\right]\right\}T, \tag{13}$$

where N_{HS} is the number of hard spheres for one mole, $\bar{R}$ is the gas constant, and $\bar{M}$ is the molar mass. The function $\Phi(f)$ represents the effect of exclude volume and f is the packing fraction (Hosono et al., 2019) (for a more detailed model of hard sphere-type equation of state, see also Wolf et al., 2015).

2.3. Variable Polytrope-Variable Grüneisen Parameter EoS by Wissing and Hobbs (2020a, 2020b)

Wissing and Hobbs (2020b) proposed equations of state that can describe the behavior of matter for both compression and expansion. They divided the phase diagram into two regions, namely compressed region ($\rho > \rho_0$) and expanded region ($\rho < \rho_0$);

$$p = \begin{cases} p_{\mathrm{co}} & (\rho > \rho_0), \\ p_{\mathrm{ex}} & (\rho < \rho_0). \end{cases} \tag{14}$$

For the compressed region, Wissing and Hobbs (2020b) adopted a variable polytrope EoS by Weppner et al. (2015). First, the isothermal pressure for the compressed region is

$$p_{\mathrm{co;iso}} = \frac{B \exp\left(\frac{A_0}{A_1}\right)}{A_1} \left[\left(\frac{\rho}{\rho_0}\right)^{A_2} \mathrm{Ei}\left(1 + \frac{A_2}{A_1}, \frac{A_0}{A_1}\left(\frac{\rho}{\rho_0}\right)^{-A_1}\right) - \mathrm{Ei}\left(1 + \frac{A_2}{A_1}, \frac{A_0}{A_1}\right)\right], \tag{15}$$

$$A_0 = B' - A_2, \tag{16}$$

$$A_1 = \frac{B'}{A_0}, \tag{17}$$

where Ei is the exponential integral

$$\mathrm{Ei}(n, x) = \int_1^\infty \frac{\exp(-xt)}{t^n} \mathrm{d}t. \tag{18}$$

The parameter B' is the pressure derivative of the bulk modulus. The parameter A_2 slightly depends on the material; however, for most materials, $A_2 = 1.95$ (Weppner et al., 2015). And, the thermal pressure is

$$p_{\mathrm{th}} = \gamma \rho u, \tag{19}$$

where γ is the Grüneisen parameter that depends on the phase and density. Wissing and Hobbs (2020b) adopted the Grüneisen parameter model given by Irvine and Stacey (1975) and Burakovsky and Preston (2004).

$$\gamma_{\mathrm{co}} = \frac{\frac{B'_{\mathrm{co;iso}}}{2} - \frac{1}{6} - \frac{t}{3}\left(1 - \frac{p_{\mathrm{co;iso}}}{3B_{\mathrm{co;iso}}}\right) - \frac{p_{\mathrm{co;iso}}}{3B_{\mathrm{co;iso}}} \rho \frac{\mathrm{d}t}{\mathrm{d}\rho}}{1 - \frac{2t}{3}\frac{p_{\mathrm{co;iso}}}{B_{\mathrm{co;iso}}}}, \tag{20}$$

$$B_{\mathrm{co;iso}} = B\left(\frac{\rho}{\rho_0}\right)^{A_2} \exp\left\{\frac{A_0}{A_1}\left[1 - \left(\frac{\rho}{\rho_0}\right)^{-A_1}\right]\right\}, \tag{21}$$

$$B'_{\mathrm{co;iso}} = A_0\left(\frac{\rho}{\rho_0}\right)^{-A_1} + A_2, \tag{22}$$

where t depends on the model of the Grüneisen parameter. Wissing and Hobbs (2020b) suggested a density-dependence model for t;

$$t = (t_{\mathrm{min}} - t_\infty)\left(\frac{\rho}{\rho_0}\right)^{-\delta_t} + t_\infty, \tag{23}$$

where t_{min} and $t_\infty (= 2.5)$ are the minimum value and the value at the infinite compression for t, respectively. The values of t_{min} and δ_t depend on materials and are given by fitting experimental data.

For the expanded region, Wissing and Hobbs (2020b) adopted the Mie potential, which is the same as ANEOS;

$$p_{\mathrm{ex;iso}} = \frac{B}{a_{\mathrm{Mie}} - b_{\mathrm{Mie}}} \left[\left(\frac{\rho}{\rho_0} \right)^{a_{\mathrm{Mie}}} - \left(\frac{\rho}{\rho_0} \right)^{b_{\mathrm{Mie}}} \right], \tag{24}$$

where a_{Mie} and b_{Mie} are power indices of the Mie potential. For the thermal pressure, Wissing and Hobbs (2020b) applied the same pressure equation to that for the compressed region but with different form of Grüneisen parameter;

$$\gamma_{\mathrm{ex}} = \gamma_k \left(\frac{\rho}{\rho_0} \right)^{c} - \left(\frac{\rho}{\rho_0} \right)^{q_0 \gamma_0 + c\gamma_k} + \gamma_{\mathrm{ideal}}, \tag{25}$$

$$\gamma_k = 1 + \gamma_0 - \gamma_{\mathrm{ideal}}, \tag{26}$$

where γ_0 is the reference Grüneisen parameter and $\gamma_{\mathrm{ideal}} = 1/3$ is a parameter to set the Grüneisen parameter at zero-density limit to that of the ideal gas.

Their approach has a merit in incorporating the variation of the Grüneisen parameter for a broad range of conditions. However, their approach has a problem similar to the problem with Stewart et al. (2020): EoS of a liquid is assumed to have a formula similar to solids where entropy is directly linked to the internal energy. In fact, the density dependence of the Grüneisen parameter follows the same trend as those of solids that is inconsistent with the experimental (and theoretical) results on silicate melts (e.g., Jing & Karato, 2011; Mosenfelder et al., 2007; Stixrude & Karki, 2005).

This problem is addressed in Wissing and Hobbs (2020b) where the unique density dependence of the Grüneisen parameter in the liquid is included. However, the exact way in which they included this important effect is not clearly described in their paper. By comparing Wissing and Hobbs (2020b) and Wissing and Hobbs (2020a), we interpret that Wissing and Hobbs (2020b) used $q \left(= \frac{\partial \log \gamma}{\partial \log V} \right) = -0.17$ that is substantially larger than the value of q in the hard-sphere model ($q = -1.5$ to -2.0; Jing and Karato (2011); Mosenfelder et al. [2007]). This makes a large difference in the degree of heating upon an impact (Karato, 2014). Also, the magma ocean assumed in Wissing and Hobbs (2020a) is much thinner (300–500 km) than in our model (1,500 km).

3. Numerical Setup

3.1. Method

In this paper, we use the smoothed particle hydrodynamics (SPH) method (Gingold & Monaghan, 1977; Lucy, 1977). This is a particle-based numerical scheme for hydrodynamic simulations. In this method, a fluid is represented as a collection of hypothetical particles, so-called SPH particles. The governing equations for fluids are converted into the sums of the interactions between two SPH particles. We also consider the self-gravity between particles. Among several formulations of SPH, we chose the Density Independent SPH (Hopkins, 2013; Hosono et al., 2013; Saitoh & Makino, 2013), a version of SPH that improves the treatment of density jump, such as the core-mantle boundary (for detailed description, see Hosono et al. [2016]). Note that Hosono et al. (2019) have already carried out runs with the standard SPH and have shown that the amount of materials ejected from the target (proto-Earth) depends strongly on the method of SPH calculation: with a standard SPH, the amount of ejected materials from the target is substantially smaller than that when DISPH is used. In the present paper, we also used these two methods for different EoS models.

Note also that the independent variables in DISPH are the density and the internal energy, so we must implicitly solve $F = U + T \left(\frac{\partial F}{\partial T} \right)_V$ (i.e., Equation 13 for the hard-sphere EoS) by U for temperature T. In this paper, we used the secant method to solve it for T (the details of the secant method can be found in textbooks of the numerical analysis, e.g., Allen & Isaacson, 1997).

Table 2
Models for Each Run

Model name	EoS for the (initial) solid mantle	EoS for the (initial) magma ocean
A	M-ANEOS	M-ANEOS
B	M-ANEOS (S+20)	M-ANEOS (S+20)
C	Wissing and Hobbs (2020b)	Wissing and Hobbs (2020b)
D	M-ANEOS (S+20)	Hard sphere (no T- nor ρ-effect)
E	M-ANEOS (S+20)	Hard sphere (+T-effect)
F	M-ANEOS (S+20)	Hard sphere (+ρ-effect)
G	M-ANEOS (S+20)	Hard sphere (+T- and ρ-effect)
H	Wissing and Hobbs (2020b)	Wissing and Hobbs (2020a)

3.2. Planetary Models and Impact Parameters

We assume that both proto-Earth and the impactor are differentiated and have 30% iron core and 70% dunite (Mg_2SiO_4) mantle. For all models, we created initial objects as per the "warm start" method given in Canup (2004); we first set up the initial condition by placing equal-mass SPH particles in the cubic lattice and then let the particles relax to the hydrostatic state. After this relaxation process has been done, we collided two objects. All models have their surface temperature greater than 2,000 K so that they have about 1,500 km magma ocean.

We consider eight models where different EoSs are used (Table 2). Table 2 summarizes the models and EoSs used for the solid mantle (both for proto-Earth and impactor) and the magma ocean. In models A, B, and C, we use the same equation of state for both (initial) magma ocean and initially solid parts. In models D, E, F, G, and H, we use different EoSs for initially solid part and initially liquid part (preexisting magma ocean).

Assuming that the escaping mass during this impact is small, we set the initial total mass in the simulations to about the current Earth mass (M_E). The masses of the target and impactor are set to $\sim 0.9 M_E$ and $\sim 0.1 M_E$. We deployed a total of 300,000 particles in all runs. Note that Hosono et al. (2017) pointed out that the results (disk mass and angular momentum) depend on the number of particles although their results are for the standard SPH. They also show that if we use greater than 300,000 particles, the results would be roughly similar. Further investigation of the number of particles with DISPH is left for future work.

The orbital angular momentum of the impactor is set to $1.2 L_{EM}$ and the impact velocity is $v_{imp} = 1.05 v_{esc}$, where L_{EM} and v_{esc} are the angular momentum in the Earth-Moon system and escape velocity, respectively. We ignored the initial rotation of both objects. The duration of this simulation is 72 hr.

3.3. Analysis

After the calculations are finished, we estimate the disk mass and composition of the disk from the simulation results (i.e., the mixing ratio of the target and the impactor in the run products). First, we classify each particle into three groups: planet, disk, and escaping particles. This is done by the method introduced by Appendix A in Canup et al. (2001). First for all particles, we check whether the particle is bounded or not by testing if the kinetic + potential energy is negative. If the particle is bounded, then we calculate the periapsis of the particle. If the periapsis is smaller than the planet's surface, then the particle is considered as a planet (target) particle. Note that we loosely estimate the planet's surface by assuming that the target has terrestrial mean density 5.5 g/cm^3. Otherwise, the particle is considered as a disk particle.

Note that this method must be iteratively solved because the planet's mass is determined by summing up the mass of the planet particles. Hence, we set the current Earth's mass to the initial guess of planet's mass and iteratively solve it.

After calculating the evolution of mass in each component, we calculated two parameters that characterize the similarity and differences in composition between the Moon (disk) and Earth. The first is a parameter defined by

$$\delta f_{tar} = f_{tar}^{E} - f_{tar}^{M}, \tag{27}$$

where $f_{tar}^{E,M}$ is the fraction of target materials in Earth (E) or in the Moon (M) (note that this definition of compositional difference (δf_{tar}) is different from that defined by Canup (2012), that is, $\delta f_T = \frac{f_{tar}^{M}}{f_{tar}^{E}} - 1$. Although they agree with each other at $f_{tar}^{E} \to 1$ (for a reason for the difference, see Hosono et al. [2019])). This parameter involves the mass fraction of a disk from the target and the impactor and is an indicator of the degree of similarity in the isotopic composition between the Moon and Earth. Hosono et al. (2019) showed that for a model to be consistent with the isotopic observations, $\delta f_{tar} < 0.15$ (for the justification of this number, see Canup [2012]).

The second one is a parameter that characterizes the difference in the FeO/(FeO + MgO) ratio $X_{\mathrm{FeO/MgO}}$ between the Moon and Earth,

$$\delta\xi_{\mathrm{FeO/MgO}} \equiv \frac{X^{\mathrm{M}}_{\mathrm{FeO/MgO}}}{X^{\mathrm{E}}_{\mathrm{FeO/MgO}}} - 1 = f^{\mathrm{M}}_{\mathrm{MO}}\left(\frac{X^{\mathrm{MO}}_{\mathrm{FeO/MgO}}}{X^{\mathrm{solid}}_{\mathrm{FeO/MgO}}} - 1\right) + f^{\mathrm{M}}_{\mathrm{imp}}\left(\frac{X^{\mathrm{imp}}_{\mathrm{FeO/MgO}}}{X^{\mathrm{solid}}_{\mathrm{FeO/MgO}}} - 1\right), \tag{28}$$

where $X^{\mathrm{M,E}}_{\mathrm{FeO/MgO}}$ is $X_{\mathrm{FeO/MgO}}$ of the Moon (M) or Earth (E), $X^{\mathrm{MO}}_{\mathrm{FeO/MgO}}$ is $X_{\mathrm{FeO/MgO}}$ of the magma ocean, $X^{\mathrm{imp}}_{\mathrm{FeO/MgO}}$ is $X_{\mathrm{FeO/MgO}}$ of the impactor, $X^{\mathrm{solid}}_{\mathrm{FeO/MgO}}$ is $X_{\mathrm{FeO/MgO}}$ of the solid part of the target, $f^{\mathrm{M}}_{\mathrm{MO}}$ is the fraction of the magma ocean materials in the disk, and $f^{\mathrm{M}}_{\mathrm{imp}}$ is the fraction of the impactor materials. Equation 28 shows that the difference in $X_{\mathrm{FeO/MgO}}$, that is, $\delta\xi_{\mathrm{FeO/MgO}}$, is controlled by the difference in the FeO/(FeO + MgO) ratio between the magma ocean and the solid part of the target $\left(\frac{X^{\mathrm{MO}}_{\mathrm{FeO/MgO}}}{X^{\mathrm{solid}}_{\mathrm{FeO/MgO}}} - 1\right)$ as well as the difference between the impactor and the solid part of the target $\left(\frac{X^{\mathrm{imp}}_{\mathrm{FeO/MgO}}}{X^{\mathrm{solid}}_{\mathrm{FeO/MgO}}} - 1\right)$. In Figure 4, we show $\delta\xi_{\mathrm{FeO/MgO}}$ for a case of $\frac{X^{\mathrm{imp}}_{\mathrm{FeO/MgO}}}{X^{\mathrm{solid}}_{\mathrm{FeO/MgO}}} - 1 = 1$ (Mars-like impactor) and $\frac{X^{\mathrm{MO}}_{\mathrm{FeO/MgO}}}{X^{\mathrm{solid}}_{\mathrm{FeO/MgO}}} - 1 = 0.7$ (a case of 20% partial melting; see Hosono et al. [2019]). A successful model should show $\delta\xi_{\mathrm{FeO/MgO}} \simeq 0.5$.

4. Results

The results of giant impact simulations are summarized in Figures 1–3. Figure 1 shows the snapshots of computational results for the early stage ($t < 19.2$ hr). The impactor hits the proto-Earth at $t = 0.6$ hr. Upon the impact, the impactor is greatly deformed and an arm-like structure is formed ($t = 1.8$–3.6 hr). Meanwhile, a clump of a remnant of the impactor is formed ($t = 6.0$–19.2 hr). The orbit of this clump depends on the EoS; however, it eventually recollides to the proto-Earth.

Figure 2 shows the final snapshots ($t = 72$ hr) for each run. After a collision, a massive disk is formed inside the Roche limit. From these figures, we can see that if the upper mantle of the proto-Earth (magma ocean) is modeled using a hard-sphere equation of state, a target-rich proto-lunar disk is formed. We can also see that the final disk mass depends on the EoS of the solid mantle. When model A (or B) is used for the magma ocean, the disk mass is smaller than for other models (see also Figure 3 where the edge-on views of the final snapshots are shown).

Figure 4 shows the time evolution of the disk mass, impactor fraction in the disk, and MO fraction in the disk. Figure 5 shows composition deviation (δf_{tar}) and the difference in the FeO/(FeO + MgO) ratio ($\delta\xi_{\mathrm{FeO/MgO}}$) for the case of a Mars-like impactor. For all runs, the final disk mass is compared to the current Moon mass. However, only the runs where hard-sphere EoS is used for the magma ocean satisfy the condition needed to explain the isotopic similarity, that is, $\delta f_{\mathrm{tar}} < 0.15$. Among the various versions of the hard-sphere EoS, the influence of temperature dependence of the hard-sphere diameter has little effects on the outcome. The density dependence of the hard-sphere diameter changes the time of sudden decrease in the compositional deviation and disk mass due to the recollision of the impactor; however, the final results are almost the same. This result is consistent with Hosono et al. (2019)'s results although we used M-ANEOS for solid mantle. In case of the hard-sphere model for magma ocean materials, the MO fraction of the disk is ∼70% and $\delta f_{\mathrm{tar}} \simeq 0.15$. In contrast, when we use Wissing and Hobbs (2020a)'s EoS for the magma ocean, even though the model contains a magma ocean, the MO fraction is only ∼40% and $\delta f_{\mathrm{tar}} \simeq 0.5$ that is too large to explain the isotopic similarity.

In the bottom row in Figure 5, we show δf_{tar} and $\delta\xi_{\mathrm{FeO/MgO}}$. The hatched regions are the successful values ($\delta f_{\mathrm{tar}} < 0.15$). For $\delta\xi_{\mathrm{FeO/MgO}}$, we loosely assume that $0.4 < \delta\xi_{\mathrm{FeO/MgO}} < 0.6$. We show $\delta\xi_{\mathrm{FeO/MgO}}$ in vertical error bar by varying $\frac{X^{\mathrm{imp}}_{\mathrm{FeO/MgO}}}{X^{\mathrm{solid}}_{\mathrm{FeO/MgO}}}$ in a plausible range (1 for an Earth-like impactor and 2 for Mars-like impactor). All models with hard-sphere EoS come close to successful region, whereas the other models have large deviation in $\delta\xi_{\mathrm{FeO/MgO}}$.

If we assume $\delta f_{\mathrm{tar}} < 0.15$ as required from the isotopic similarity, all models without magma ocean fail to explain the observed difference in the FeO/(FeO + MgO) ratio because in order to explain $\delta\xi_{\mathrm{FeO/MgO}} \simeq 0.5$ without magma ocean contribution, we need to assume $\frac{X^{\mathrm{imp}}_{\mathrm{FeO/MgO}}}{X^{\mathrm{solid}}_{\mathrm{FeO/MgO}}} \simeq 4$, that is highly unlikely ($\frac{X^{\mathrm{imp}}_{\mathrm{FeO/MgO}}}{X^{\mathrm{solid}}_{\mathrm{FeO/MgO}}} \simeq 2$ for Mars). Since the isotopic similarity requires $\delta f_{\mathrm{tar}} < 0.15$, contribution from the possible compositional difference of the impactor

10.1029/2021JE006971

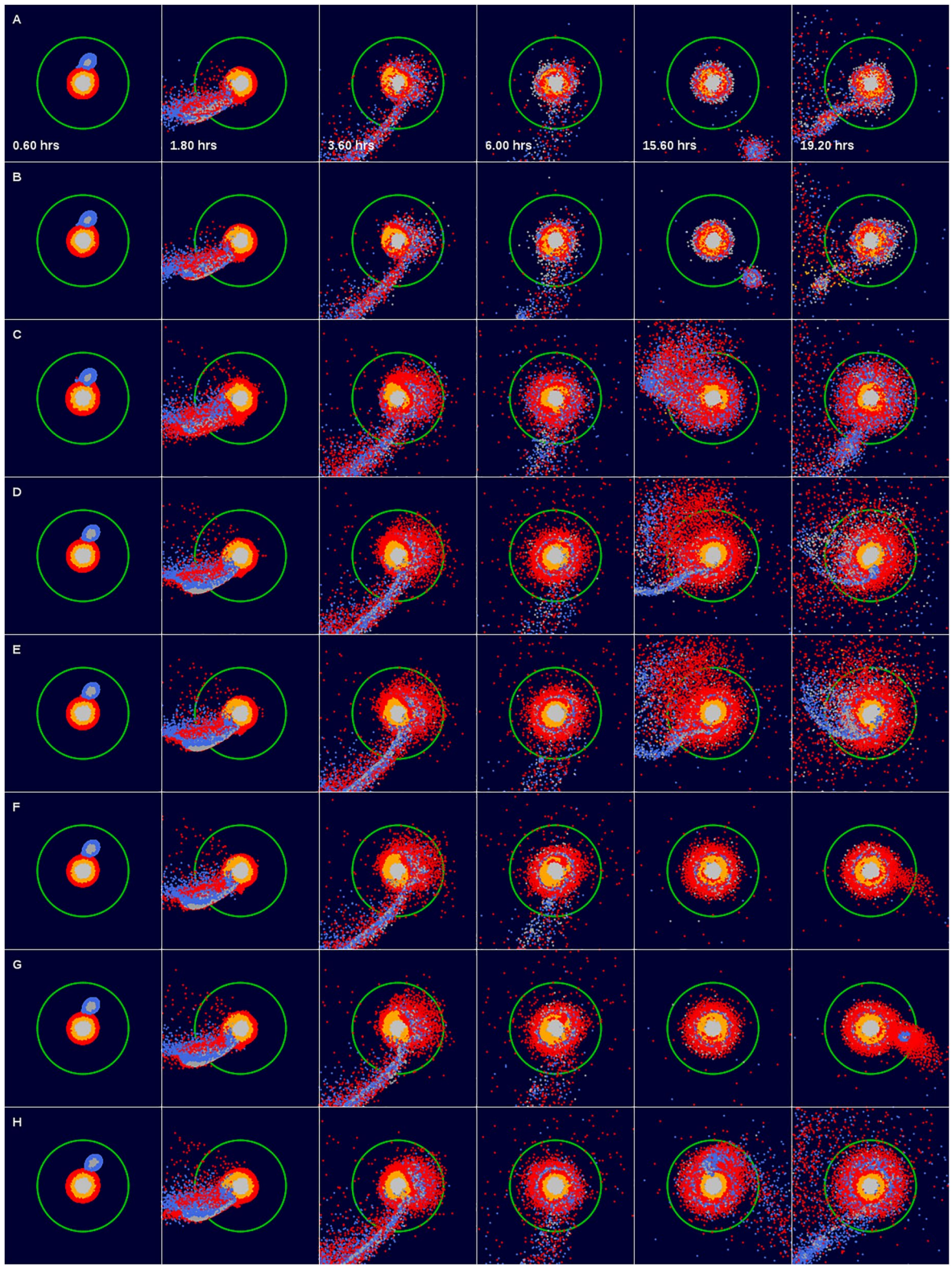

Figure 1. Each panel displays the distribution of SPH particles of each run. The model names are shown in the top-left corner. The red, orange, gray, blue, and dark-gray particles are particles that are initially in the target's preexistence magma ocean, target's solid mantle, target's core, impactor's mantle, and impactor's core, respectively. The green circles indicate the Roche limit ($2.9R_E$).

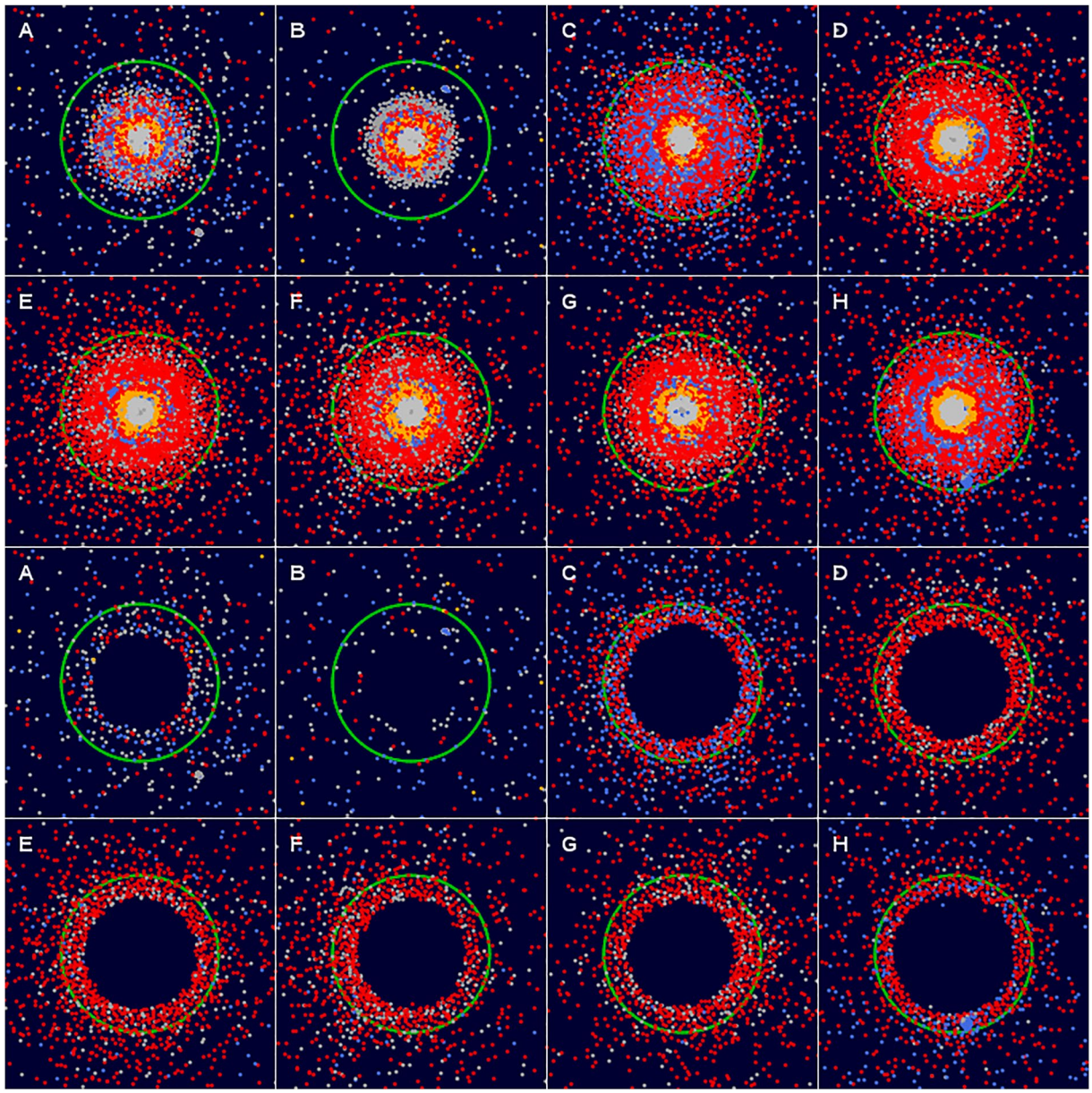

Figure 2. Snapshots at the end of the simulations (72 hr) are shown. The color of each particle is the same as Figure 1. Upper two rows show all particles, whereas the lower two rows show only disk particles.

is small. For a plausible range of $\frac{X^{\rm imp}_{\rm FeO/MgO}}{X^{\rm solid}_{\rm FeO/MgO}}$ (= 1–2), $\delta\xi_{\rm FeO/MgO} \simeq 0.5$ can be explained by the FeO-rich magma ocean with $\frac{X^{\rm MO}_{\rm FeO/MgO}}{X^{\rm solid}_{\rm FeO/MgO}} \simeq 1.5 - 1.7$ corresponding to ∼20–40% of partial melting (Hosono et al., 2019).

From these results, we conclude that when we use the EoS proposed by Stewart et al. (2020) or Wissing and Hobbs (2020b); Wissing and Hobbs (2020a), the GI with the given collision conditions cannot produce a disk (the Moon) whose isotopic composition is similar to Earth. The run with hard-sphere EoS could satisfy isotopic similarity as well as the difference in FeO/(FeO + MgO) ratio, regardless of the choice of the parameters (η and ξ). Recall that Hosono et al. (2019) used Tillotson EoS, whereas in this paper, we used M-ANEOS for the solid mantle. Hence, the choice of the EoS for the solid mantle does not play an important role for the compositional deviation. Finally, the choice of the EoS for the MO plays an important role. The hard-sphere EoS satisfies the compositional deviation ($\delta f_{\rm tar} < 0.15$) and the FeO/(FeO + MgO) ratio ($\delta\xi_{\rm FeO/MgO} \simeq 0.5$), whereas the solid-like EoSs (Stewart et al., 2020; Wissing & Hobbs, 2020a, 2020b) do not.

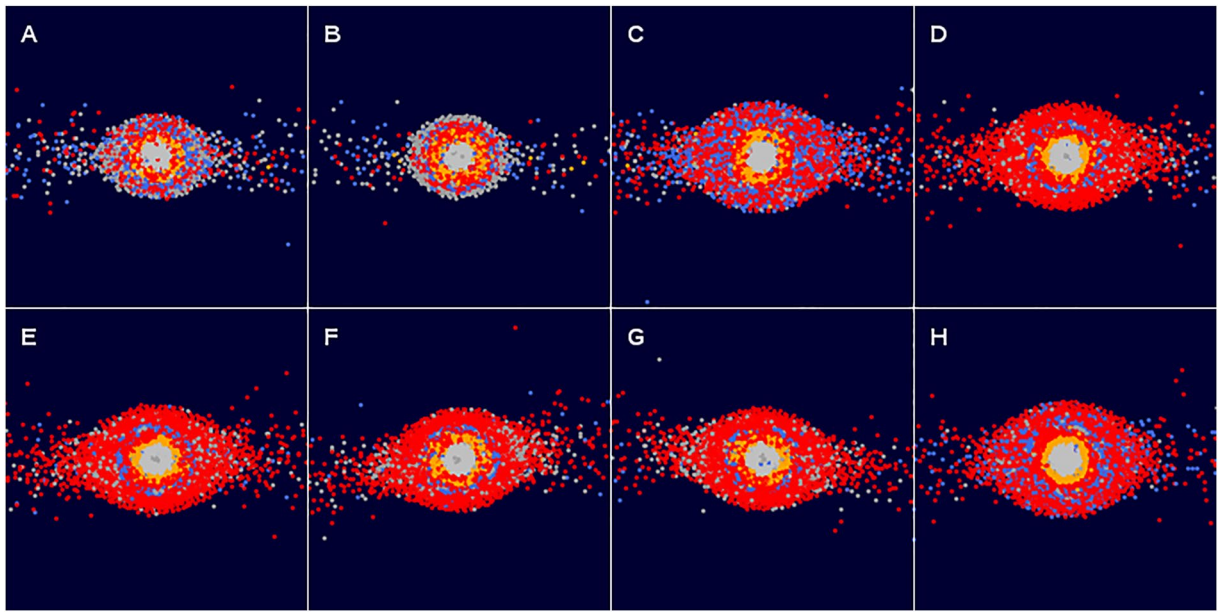

Figure 3. Same as Figure 2 but shows edge-on view of all particles.

Pahlevan et al. (2011) proposed an alternative model where they emphasize the extensive chemical reactions between the magma ocean on Earth and the Moon-forming disk. Such a process may operate and provide an additional mechanism to explain the inferred high FeO/(FeO + MgO) ratio of the Moon. However, the degree to which such a process can explain the Moon's composition is unclear (e.g., Melosh, 2014).

5. Summary and Discussion

Since a giant impact produces a vast range of pressure and temperature, treating thermodynamic properties over a broad range of conditions, including phase transformation, is essential. However, most of the previous studies that considered only limited aspects, such as the latent heat upon vapourization (e.g., Melosh, 2007) and the role of melts (preexisting magma ocean), were largely ignored.

Karato (2014) and Hosono et al. (2019) demonstrated the importance of unique thermodynamic properties of silicate melts in controlling the fate of a giant impact. However, there have been a few new papers on the issues of EoS in a giant impact (e.g., Stewart et al., 2020; Wissing & Hobbs, 2020b, 2020a) that presented somewhat different EoSs and pointed out a problem in Hosono et al. (2019)'s treatment of EoS across the solid vapor transition.

In response to these new results, we explored the influence of various EoSs on the consequence of a giant impact and obtained the following results:

1. The modification of Tillotson EoS to M-AMEOS for the solid part of the target in the model explored by Hosono et al. (2019) has a minor effect on the results. In both cases, the disk contains a substantially larger amount of target materials in comparison to other models.
2. We also explored the influence of more realistic EoS for the silicate melts that include the variation of the hard-sphere size with temperature and density. Our results show that those modifications have relatively small effects on the composition of the disk.
3. If the EoS proposed by Stewart et al. (2020) is used to the preexisting magma ocean, the disk is made largely of the impactor materials that are not consistent with the observation. This is true even if we use DISPH.
4. If the EoS proposed by Wissing and Hobbs (2020a) is used for the preexisting magma ocean, the fraction of target materials is larger than the model using EoS by Stewart et al. (2020).
5. However, the disk formed using the EoS by Wissing and Hobbs (2020a) still contains a substantial fraction of the impactor (~50%; Figure 4).

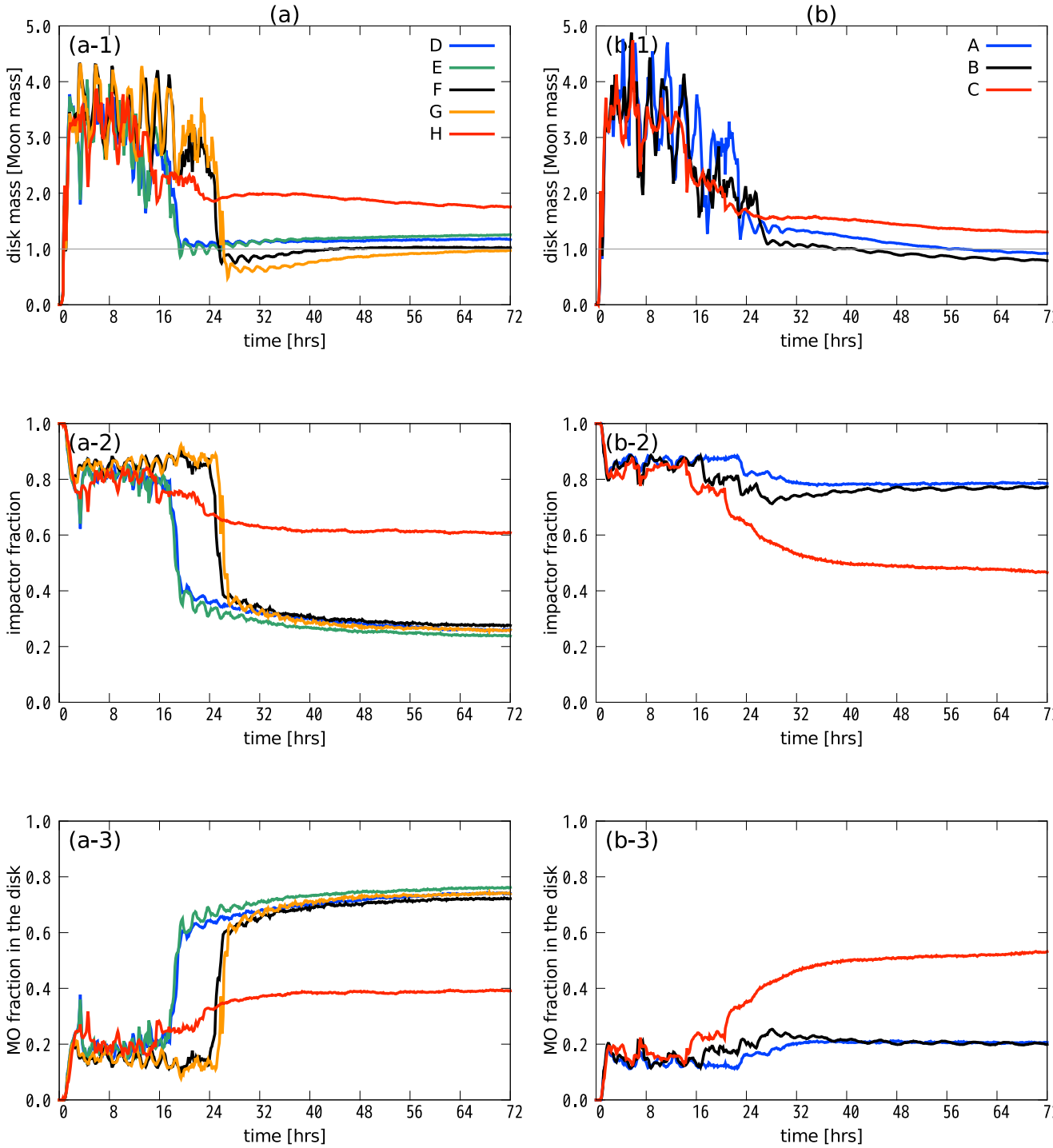

Figure 4. Time evolution for the disk mass normalized by the current Moon mass, impactor fraction in the disk, magma ocean fraction in the disk from top to bottom, respectively. The left column shows the results of models that use the same EoS to both initially solid and liquid part, whereas the right column shows those of models that use different EoSs to initially solid and liquid parts.

Point (1) (the insensitivity of the results on the choice of EoS for a region i.e., initially solids) indicates that the presence of a magma ocean in the target (proto-Earth) is a key in controlling the composition of the disk.

Point (2) shows that a more realistic deformable sphere model of EoS for silicate melts also results in the disk composition that is consistent with the observed composition of the Moon.

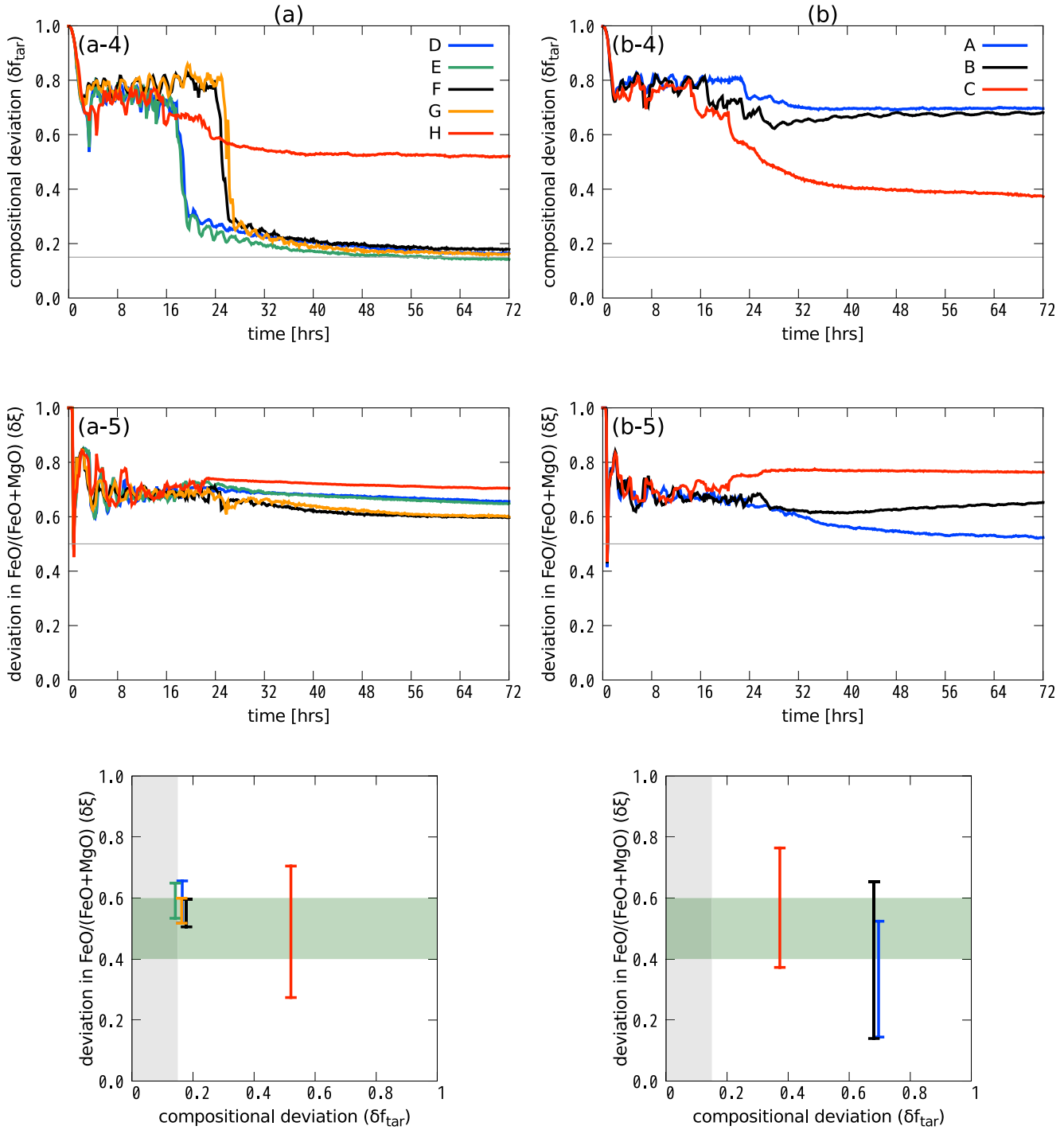

Figure 5. Top two rows show the time evolution of the composition deviation and deviation in FeO/(FeO + MgO) for models with and without magma ocean. The bottom row shows $\delta f_{\rm tar}$ versus $\delta\xi_{\rm FeO/(MgO+FeO)}$ at $t = 72$ hr. The hatched regions are a successful range for these compositions. The vertical error bar is given by varying $\frac{X^{\rm imp}_{\rm FeO/MgO}}{X^{\rm solid}_{\rm FeO/MgO}}$ in a plausible range.

Points (3) and (4) demonstrate the importance of a magma ocean. In this context, we may note that the EoS proposed by Stewart et al. (2020) also include the liquid state. Therefore, it is important to understand why the use of Stewart et al. (2020)'s EoS results in largely different composition of the disk from our model. There are two reasons for this: (a) in a model with the Stewart et al. (2020) EoS, we do not assume the presence of a magma

ocean in the target. In such a case, formation of a magma ocean consumes energy and reduces the heating and the amount of target materials to become a part of the disk. (b) Although Stewart et al. (2020)'s EoS includes a liquid state, their EoS does not include the contribution of the configurational entropy that is a key property of a silicate melt.

Point (5) shows that the details of EoS of the magma ocean matter. Wissing and Hobbs (2020b); Wissing and Hobbs (2020a)'s EoS includes important details on the behavior of the Grüneisen parameter. However, their EoS does not capture the important role of configurational entropy. We believe that this is a reason why the results using Wissing and Hobbs (2020b); Wissing and Hobbs (2020a) EoS differ from the results using the hard-sphere (or the deformable sphere) EoS.

Regarding the composition of the Moon (disk) predicted by various models, we conclude:

1. The similarity in the isotopic composition can be explained if $\delta f_{\rm tar} < 0.15$ and this condition is met if we use a hard-sphere EoS including the modified one for the magma ocean.
2. If we use a conventional collision condition, this condition ($\delta f_{\rm tar} < 0.15$) cannot be obtained using other EoSs where the role of configurational entropy is not included.
3. Given the requirement of $\delta f_{\rm tar} < 0.15$, the possible contribution from the impactor to modify $X_{\rm FeO/MgO}$ of the Moon (disk) away from that of Earth is difficult because if deviation in $X_{\rm FeO/MgO}$ comes only from the composition of the impactor, this will require unrealistically large $X_{\rm FeO/MgO}$ for an impactor.

Obviously, if one chooses other unconventional collision conditions, such as the head-on collision with high collision velocity, then the impactor and the target will be mixed well and one would be able to explain the similarity in the isotopic composition (e.g., Canup, 2012; Lock et al., 2018). However, the problems with those models are the low probability of such collisions and that it is not clear how these models explain the difference in the FeO/(FeO + MgO) ratio.

We may also note that magma ocean may not have to exist before a collision. A high-energy collision will deliver large energy, and melting (and even vapourization) would occur as a result of the collision. The results similar to the present study may be obtained in such a case. However, since melting consumes energy by the latent heat, the efficiency of bringing magma ocean materials to the disk will be less than a case of preexisting magma ocean. This issue needs to be examined. Similarly, the collision conditions (angular momentum, impact velocity, and impactor mass) that we have explored (Hosono et al. (2019) and this study) are limited. Further studies will be important to explore a broader range of collision conditions.

Note that upon a giant impact, some of the preexisting solids will melt (or even vapourized) (e.g., Nakajima et al., 2021). Consequently, it is important to follow the *p*-*T*-density path of materials through a giant impact and use EoS appropriate for each phase. In the present study, we did this in a simplified manner to use M-ANEOS for the initially solid parts that contain an influence of a phase transition from a solid to a gas but not a solid to liquid transition. By doing this, we underestimate the role of melting in the initially solid parts because M-ANEOS EoS does not capture the thermodynamic properties of silicate melts. However, this simplified approach can be justified because the amount of melt formed in the initially solid parts is small compared to the preexisting magma ocean (1,500 km thickness is assumed). This is due to the fact that upon a collision of preexisting melt (magma ocean) and solid impactor, a majority of heating occurs in the preexisting liquid and not much in the solid because of the large difference in the thermodynamic properties as shown by Karato (2014). In fact, in the simulations performed in this paper, only about 20% of the solid mantle would melt after the impact (as compared to ∼70% calculated by Nakajima et al. [2021]). Therefore, the mass of the melt formed from the solid by a giant impact is ∼10% of the mass of the preexiting magma ocean.

The use of this simplified approach would result in the underestimate of the target mass in the disk. In other words, our simplified simulations would provide the minimum value for the target fraction and therefore, the use of a more complicated EoS for the initially solid parts will support our conclusion of a large fraction of the target mass even more strongly. In any case, the degree of underestimate would be small because of a small amount of impact-induced melt compared to the preexisting magma ocean.

We also note that the net amount of melt produced in (Nakajima et al., 2021) model is not very different from the net amount of melt in our model. Nevertheless, the consequence of a giant impact for the disk composition is largely different. This is due to the different EoSs were used in these two studies.

We conclude that including the unique thermodynamic properties of silicate melt (magma ocean) is critical in understanding the composition of the Moon-forming disk (and the Moon). If we accept the presence of magma ocean in the target (growing Earth in its later stage of formation) (e.g., Abe & Matsui, 1985; Sasaki & Nakazawa, 1986) and use an EoS appropriate for silicate melts (magma ocean), the compositional similarities (isotopic ratios) and differences (FeO/(FeO + MgO)) between the Moon and Earth can be explained without invoking rare collision conditions, such as a head-on collision of similar mass planets or an extremely high energy collision (Canup et al., 2021). Because the presence of a magma ocean in many terrestrial planets is likely in its later stage of formation and because the canonical collision conditions are common compared to extreme conditions considered by other studies (see Canup et al. [2021]), we conclude that the formation of the Moon as we observe for Earth is not so a rare event.

Data Availability Statement

The codes used for generating the tables of M-ANEOS in this study are preserved at https://zenodo.org/record/3478631 (Stewart et al., 2019) and https://zenodo.org/record/3525030 (Thompson et al., 2019).

Acknowledgments
This paper is dedicated to late Jay Melosh who gave us a lot of inspirations and encouragements based on rigorous and fair criticisms. We thank Dr. Gareth Collins and anonymous reviewer for carefully reading our manuscript and giving us insightful comments. This work was supported by JSPS KAKENHI Grant No. 19K14826. The tabulated M-ANEOS supporting the study is generated by Thompson et al. (2019) and Stewart et al. (2019).

References

Abe, Y., & Matsui, T. (1985). The formation of an impact-generated H_2O atmosphere and its implications for the early thermal history of the Earth. *Journal of Geophysical Research*, *90*(S02), C545–C559. Retrieved from https://agupubs.onlinelibrary.wiley.com/doi/abs/10.1029/JB090iS02p0C545

Allen, M., & Isaacson, E. (1997). *Numerical analysis for applied science*. Wiley. Retrieved from https://books.google.co.jp/books?id=PpB9cjOxQAQC

Anderson, O. L. (1996). *Equations of state of solids for geophysics and ceramic science*.

Burakovsky, L., & Preston, D. L. (2004). Analytic model of the Gruneisen parameter all densities. *Journal of Physics and Chemistry of Solids*, *65*(8–9), 1581–1587. https://doi.org/10.1016/j.jpcs.2003.10.076

Canup, R. M. (2004). Simulations of a late lunar-forming impact. *Icarus*, *168*(2), 433–456. https://doi.org/10.1016/j.icarus.2003.09.028

Canup, R. M. (2012). Forming a Moon with an Earth-like composition via a giant impact. *Science*, *338*(6110), 1052–1055. https://doi.org/10.1126/science.1226073

Canup, R. M. (2014). Lunar-forming impacts: Processes and alternatives. *Philosophical Transactions of the Royal Society of London,Series A*, *372*(2024), 20130175. https://doi.org/10.1098/rsta.2013.0175

Canup, R. M., & Asphaug, E. (2001). Origin of the Moon in a giant impact near the end of the Earth's formation. *Nature*, *412*(6848), 708–712. https://doi.org/10.1038/35089010

Canup, R. M., Righter, K., Dauphas, N., Pahlevan, K., Ćuk, M., Lock, S. J., et al. (2021). *Origin of the Moon*. arXiv e-prints, arXiv:2103.02045.

Canup, R. M., Ward, W. R., & Cameron, A. G. W. (2001). A scaling relationship for satellite-forming impacts. *Icarus*, *150*(2), 288–296. https://doi.org/10.1006/icar.2000.6581

Elkins-Tanton, L. T. (2013). Planetary science: Occam's origin of the Moon. *Nature Geoscience*, *6*(12), 996–998. https://doi.org/10.1038/ngeo2026

Gingold, R. A., & Monaghan, J. J. (1977). Smoothed particle hydrodynamics: Theory and application to non-spherical stars. *Monthly Notices of the Royal Astronomical Society*, *181*(3), 375–389. https://doi.org/10.1093/mnras/181.3.375

Halliday, A. N. (2012). The origin of the moon. *Science*, *338*(6110), 1040–1041. Retrieved from https://science.sciencemag.org/content/338/6110/1040

Hopkins, P. F. (2013). A general class of Lagrangian smoothed particle hydrodynamics methods and implications for fluid mixing problems. *Monthly Notices of the Royal Astronomical Society*, *428*(4), 2840–2856. https://doi.org/10.1093/mnras/sts210

Hosono, N., Iwasawa, M., Tanikawa, A., Nitadori, K., Muranushi, T., & Makino, J. (2017). Unconvergence of very-large-scale giant impact simulations. *Publications of the Astronomical Society of Japan*, *69*(2), 26. https://doi.org/10.1093/pasj/psw131

Hosono, N., Karato, S.-i., Makino, J., & Saitoh, T. R. (2019). Terrestrial magma ocean origin of the Moon. *Nature Geoscience*, *12*(6), 418–423. https://doi.org/10.1038/s41561-019-0354-2

Hosono, N., Saitoh, T. R., & Makino, J. (2013). *Density-Independent Smoothed Particle Hydrodynamics for a Non-ideal Equation of State*. Publications of the Astronomical Society of Japan, Vol. 65(5), pp. 108. https://doi.org/10.1093/pasj/65.5.108

Hosono, N., Saitoh, T. R., Makino, J., Genda, H., & Ida, S. (2016). The giant impact simulations with density independent smoothed particle hydrodynamics. *Icarus*, *271*, 131–157. https://doi.org/10.1016/j.icarus.2016.01.036

Irvine, R. D., & Stacey, F. D. (1975). Pressure dependence of the thermal grüneisen parameter, with application to the Earth's lower mantle and outer core. *Physics of the Earth and Planetary Interiors*, *11*(2), 157–165. Retrieved from http://www.sciencedirect.com/science/article/pii/0031920175900096

Jing, Z., & Karato, S.-i. (2011). A new approach to the equation of state of silicate melts: An application of the theory of hard sphere mixtures. *Geochimica et Cosmochimica Acta*, *75*(22), 6780–6802. https://doi.org/10.1016/j.gca.2011.09.004

Karato, S.-i. (2014). Asymmetric shock heating and the terrestrial magma ocean origin of the Moon. *Proceeding of the Japan Academy, Series B*, *90*(3), 97–103. https://doi.org/10.2183/pjab.90.97

Lebowitz, J. L., Helfand, E., & Praestgaard, E. (1965). Scaled particle theory of fluid mixtures. *The Journal of Chemical Physics*, *43*(3), 774–779. https://doi.org/10.1063/1.1696842

Lock, S. J., Stewart, S. T., Petaev, M. I., Leinhardt, Z., Mace, M. T., Jacobsen, S. B., & Cuk, M. (2018). The origin of the moon within a terrestrial synestia. *Journal of Geophysical Research: Planets*, *123*(4), 910–951. https://doi.org/10.1002/2017je005333

Lucy, L. B. (1977). A numerical approach to the testing of the fission hypothesis. *The Astronomical Journal*, *82*, 1013–1024. https://doi.org/10.1086/112164

Melosh, H. J. (2007). A hydrocode equation of state for sio2. *Meteoritics & Planetary Sciences*, *42*(12), 2079–2098. Retrieved from https://onlinelibrary.wiley.com/doi/abs/10.1111/j.1945-5100.2007.tb01009.x

Melosh, H. J. (2014). New approaches to the moon's isotopic crisis. *Philosophical Transactions of the Royal Society A: Mathematical, Physical & Engineering Sciences*, *372*(2024), 20130168. Retrieved from https://royalsocietypublishing.org/doi/abs/10.1098/rsta.2013.0168

Mosenfelder, J. L., Asimow, P. D., & Ahrens, T. J. (2007). Thermodynamic properties of mg2sio4 liquid at ultra-high pressures from shock measurements to 200 gpa on forsterite and wadsleyite. *Journal of Geophysical Research*, *112*(B6). Retrieved from https://agupubs.onlinelibrary.wiley.com/doi/abs/10.1029/2006JB004364

Nakajima, M., Golabek, G. J., Wünnemann, K., Rubie, D. C., Burger, C., Melosh, H. J., et al. (2021). Scaling laws for the geometry of an impact-induced magma ocean. *Earth and Planetary Science Letters*, *568*, 116983. Retrieved from https://www.sciencedirect.com/science/article/pii/S0012821X21002429

Pahlevan, K., Stevenson, D. J., & Eiler, J. M. (2011). Chemical fractionation in the silicate vapor atmosphere of the Earth. *Earth and Planetary Science Letters*, *301*(3), 433–443. Retrieved from https://www.sciencedirect.com/science/article/pii/S0012821X10006795

Rivers, M. L., & Carmichael, I. S. E. (1987). Ultrasonic studies of silicate melts. *Journal of Geophysical Research*, *92*(B9), 9247–9270. https://doi.org/10.1029/JB092iB09p09247

Saitoh, T. R., & Makino, J. (2013). A density-independent formulation of smoothed particle hydrodynamics. *The Astrophysical Journal*, *768*(1), 44. https://doi.org/10.1088/0004-637X/768/1/44

Sakai, R., Nagahara, H., Ozawa, K., & Tachibana, S. (2014). Composition of the lunar magma ocean constrained by the conditions for the crust formation. *Icarus*, *229*, 45–56. Retrieved from https://www.sciencedirect.com/science/article/pii/S0019103513004600

Sasaki, S., & Nakazawa, K. (1986). Metal-silicate fractionation in the growing Earth: Energy source for the terrestrial magma ocean. *Journal of Geophysical Research*, *91*(B9), 9231–9238. Retrieved from https://agupubs.onlinelibrary.wiley.com/doi/abs/10.1029/JB091iB09p09231

Stevenson, D. J. (1987). Origin of the moon-the collision hypothesis. *Annual Review of Earth and Planetary Sciences*, *15*(1), 271–315. https://doi.org/10.1146/annurev.ea.15.050187.001415

Stewart, S., Davies, E., Duncan, M., Lock, S., Root, S., Townsend, J., et al. (2020). The shock physics of giant impacts: Key requirements for the equations of state. *AIP Conference Proceedings*, *2272*(1), 080003. Retrieved from https://aip.scitation.org/doi/abs/10.1063/12.0000946

Stewart, S. T., Davies, E. J., Duncan, M. S., Lock, S. J., Root, S., Townsend, J. P., et al. (2019). Equation of state model forsterite-ANEOS-SLVTv1.0G1: Documentation and comparisons. *Zenodo*. https://doi.org/10.5281/zenodo.3478631

Stixrude, L., & Karki, B. (2005). Structure and freezing of mgsio$_3$ liquid in Earth's lower mantle. *Science*, *310*(5746), 297–299. Retrieved from https://www.science.org/doi/abs/10.1126/science.1116952

Thiele, E. (1963). Equation of state for hard spheres. *The Journal of Chemical Physics*, *39*(2), 474–479. https://doi.org/10.1063/1.1734272

Thompson, S. L., Lauson, H. S., Melosh, H. J., Collins, G. S., & Stewart, S. T. (2019). M-aneos. *Zenodo*. https://doi.org/10.5281/zenodo.3525030

Tillotson, J. H. (1962). Metallic equations of state for hypervelocity impact. Technical Report. *General Atomic Report GA-3216*.

Weppner, S. P., McKelvey, J. P., Thielen, K. D., & Zielinski, A. K. (2015). A variable polytrope index applied to planet and material models. *Monthly Notices of the Royal Astronomical Society*, *452*(2), 1375–1393. https://doi.org/10.1093/mnras/stv1397

Wissing, R., & Hobbs, D. (2020a). A new equation of state applied to planetary impacts. I. Models of planetary interiors. *Astronomy & Astrophysics*, *635*, A21. https://doi.org/10.1051/0004-6361/201935814

Wissing, R., & Hobbs, D. (2020b). A new equation of state applied to planetary impacts - II. Lunar-forming impact simulations with a primordial magma ocean. *Astronomy & Astrophysics*, *643*, A40. https://doi.org/10.1051/0004-6361/201936227

Wolf, A. S., Asimow, P. D., & Stevenson, D. J. (2015). Coordinated hard sphere mixture (chasm): A simplified model for oxide and silicate melts at mantle pressures and temperatures. *Geochimica et Cosmochimica Acta*, *163*, 40–58. Retrieved from https://www.sciencedirect.com/science/article/pii/S0016703715002240